



CT&F - Ciencia, Tecnología y Futuro

ISSN: 0122-5383

Instituto Colombiano del Petróleo (ICP) - ECOPETROL S.A.

Jiménez, Anyeres A; Muñoz-Cuartas, J. C; Avendaño, Sheryl
INTEGRAL MODELLING OF PROPAGATION OF INCIDENT WAVES IN A
LATERALLY VARYING MEDIUM: AN EXPLORATION IN THE FREQUENCY DOMAIN
CT&F - Ciencia, Tecnología y Futuro, vol. 8, no. 2, 2018, July-December, pp. 33-45
Instituto Colombiano del Petróleo (ICP) - ECOPETROL S.A.

DOI: <https://doi.org/10.29047/01225383.79>

Available in: <https://www.redalyc.org/articulo.oa?id=46558134003>

- How to cite
- Complete issue
- More information about this article
- Journal's webpage in redalyc.org

redalyc.org

Scientific Information System Redalyc
Network of Scientific Journals from Latin America and the Caribbean, Spain and
Portugal

Project academic non-profit, developed under the open access initiative

ARTICLE INFO:

Received : April 30, 2018

Revised : August 27, 2018

Accepted : October 16, 2018

CT&F - Ciencia, Tecnología y Futuro Vol 8, Num 2 Dec. 2018. pages 33 - 45

DOI : <https://doi.org/10.29047/01225383.79>

INTEGRAL MODELLING OF PROPAGATION OF INCIDENT WAVES IN A Laterally VARYING MEDIUM: AN EXPLORATION IN THE FREQUENCY DOMAIN

■ **MODELADO INTEGRAL
DE PROPAGACIÓN DE
ONDAS INCIDENTES
EN MEDIOS CON
GRADIENTES
LATERALES: UNA
EXPLORACIÓN EN
EL DOMINIO DE LA
FRECUENCIA.**

Jiménez, Anyeres A.^{a*}; Muñoz-Cuartas, J. C^a; Avendaño, Sheryl^a.

ABSTRACT

In this work we present a formalism that intends to solve the problem of modeling wave propagation in the context of seismic inversion. The formalism is based on the linear perturbation theory of Cauchy's equations. Based on the foregoing, we derived an equivalent Helmholtz equation for the propagation of waves in a variable density media. Then, we defined a solution, by using the boundary conditions on a half plane. This solution is of an integral nature and resembles expansion in a Neumann series. We implemented the solution of the first terms in the series, considering only the incident wavefield and neglecting the reflections. We show how this approximation works in different media that include lateral inhomogeneities in the velocity. The method presented hereunder is intended as a first step in the modelling process for the full wavefield, to be used in seismic inversion methods, Full Waveform Inversion, for example.

RESUMEN

En esta investigación presentamos un formalismo que pretende contribuir al modelado de la propagación de ondas en el contexto de la inversión sísmica. El formalismo está basado en la teoría de perturbaciones lineales a las ecuaciones de Cauchy. Basados en este procedimiento derivamos una versión de la ecuación de Helmholtz que describe la propagación de ondas en un medio con densidad variable. Luego hallamos una solución en la cual se emplean condiciones de frontera de un plano semi infinito. Tal solución es expresada en forma de integral y recuerda la expansión

en series de Neumann. Nosotros implementamos la solución del primer término de la serie, que considera únicamente el campo de onda incidente, sin considerar las reflexiones de onda. Mostramos que esta aproximación funciona en diferentes medios que incluyen variaciones inhomogeneidades laterales en el perfil de velocidad. Este método es presentado como un primer paso en el proceso de modelado del campo de onda completo el cual puede ser usado en métodos de inversión sísmica tales como "Inversión de onda completa", Full Waveform Inversion, (FWI).

KEYWORDS / PALABRAS CLAVE

Neumann series | Wave propagation | Perturbative solutions | Frequency domain.

Series de Neumann | Propagación ondulatoria | Soluciones perturbativas | Dominio de la Frecuencia.

AFFILIATION

^aInstituto de Física, Facultad de Ciencias Exactas y Naturales, Universidad de Antioquia, Calle 70 No. 52-21, Medellín, Colombia
*email: anyeres.atehortua@udea.edu.co

1 INTRODUCTION

Physical properties of a medium are usually studied through the measurement of the medium's response to physical perturbations. In particular, some mechanical properties are often studied through the measurement of the response of the medium to the propagation of waves, as it is the case for seismic exploration of the subsurface.

In general, procedures to study the structure of the subsurface using as input the data collected from perturbations of the field at the surface require a way to model the propagation of waves through the medium. Together with such modeling, inversion of the modeled data is required for accessing the inferred structure of the subsurface. One of such methods that in recent years has caught attention of the academic community and industry is FWI (Full Waveform Inversion) [1]. In FWI, full wave propagation is modeled in the media and sophisticated inversion techniques are used to recover as much information as possible from the subsurface.

FWI uses forward modeling of the seismic measurement and makes a comparison of this with the residual wavefield back propagated, in order to iteratively build a final velocity model, which can provide better detail than tomographic ray-tracing approaches [1]-[2]. However, FWI depends on a good description of the wave propagation, which is framed entirely by the modeling. In this scenario, forward modeling becomes one of the most important ingredients in any implementation of FWI. One then needs a high precision tool to model wave propagation; however, usually the computational load required for such high precision is too large for practical purposes [3]. Inexpensive, high quality solutions of the wave propagation problem for FWI are issues that must be addressed if the strategy is to become feasible for the requirements of current seismic exploration.

Modeling energy propagation in the subsurface can be performed by solving Cauchy's equations [4], if the perturbations are small so as to not causing changes in the physical properties of the media such as the bulk modulus $k_b(\vec{x})$ at any position $\vec{x}=(z,x)$. Solutions to this problem, for example through, a perturbative method, can lead to alternative ways (different to the classical finite difference approach) that can provide the quality and computational efficiency that may compete with classical strategies.

In this work we propose perturbative solutions to Cauchy's equations for a media with variable density in the frequency domain. We will refer to these solutions as integral solutions (IS). Such solutions are functions that can be evaluated at each point by making integrals over the boundary of the volume used to model the subsurface. Considering the simplest seismic exploration situation, in this work we model the subsurface as a half plane in 2D.

We show numerical solutions of the problem and study its properties. Besides their potential advantages from a theoretical point of view, one of the advantages of the integral solutions is that handling this kind of problems is usually more stable numerically and provides a simpler way for using parallelization strategies.

In order to present our work, this paper is organized as follows: First, we present in section 2 the formulation of the problem and the theoretical foundations. Next, we show in section 3 the solution proposed to the problem. In section 4, we show the numerical solution to the problem and our implementation strategy. In section 5, we show the results of our computational experiments and finally, in section 6, we present our conclusions.

2. THEORETICAL FRAME

Let us consider energy propagation inside a medium with variable density. The energy is released with intensity (I) from a set of point sources. Such intensity is low enough to leave unaltered physical properties as bulk modulus k_b , but large enough to produce waves that propagate through the medium. Such energy propagation must be described by Cauchy's equations plus an equation of state [5]. We focused on situations for which the displacement of the particles constituting the medium move around its equilibrium position and, therefore, the deviatoric term in Cauchy's equations can be neglected.

In this work, the pressure field is approached through a perturbative expansion, following the ideas of [6] and [7]. In the perturbative approach, the injection of energy from the perturbation induces a displacement in the positions of the particles, which in turn induces changes in other media variables, such as density, pressure, etc. Then, in the regime of small perturbations (linear theory), quantities like the displacement vector between particles, particle velocity, density, body forces and pressure field are decomposed as the sum of functions up to first and second order. The pressure field, for instance, is expressed as

$$P(\vec{x}, t) = P^0(\vec{x}, t) + \epsilon P^1(\vec{x}, t), \quad (1)$$

where $\epsilon < 1$ represents a perturbative parameter. $P^1(\vec{x}, t)$ is understood as a small deviation from the background pressure $P^0(\vec{x}, t)$. The density function $\rho(\vec{x})$ can be written with a perturbation expansion as the Equation 1, $\rho(\vec{x}, t) = \rho^0(\vec{x}, t) + \epsilon \rho^1(\vec{x}, t)$, where $\rho^0(\vec{x})$ is the density function describing the medium up to zeroth order.

With all these ideas in mind, a formal deduction is possible from the Helmholtz equation (see [6] or [7]) the Cauchy's equations following three steps: (a) Writing the perturbative expansion (analogous to Equation 1) of the pressure, density, particle velocities in the medium, and wave sources. Then inserting such expansions in the Cauchy equations. These equations are taken with sources symbolized by an impulsive function f . (b) Changing the pressure field to an auxiliary variable $q^i(\vec{x}, t) = P^i(\vec{x}, t) / \sqrt{\rho^0(\vec{x})}$, for $i=0,1$. (c) Making a Fourier transform from t to ω . This procedure demands much algebra, but the final result are two Helmholtz equations, for the transformed fields $q^i(\vec{x}, \omega)$, for $i=0,1$, describing the energy propagation in a medium with variable density and in the frequency domain,

$$[\nabla^2 + k^i(\vec{x}, \omega)]q^i(\vec{x}, \omega) = F_{q^i}(\vec{x}, \omega), \text{ for } i=0,1. \quad (2)$$

The vector $k^i(\vec{x}, \omega) = \omega^2/c^2(\vec{x}) + \alpha^i(\vec{x})$, for $i=0,1$, plays the role of a square magnitude of a modified wave-vector. $c^2(\vec{x})$ is the wave velocity field

propagating at frequency ω . The factor $\alpha^i(\vec{x})$, having units of squared wave vector $|\vec{k}|^2$, can be understood as a dispersive term [7].

In Equation 2, we have that

$$\alpha^1(\vec{x}) = -\frac{\nabla^2 \sqrt{\rho^0(\vec{x})}}{\sqrt{\rho^0(\vec{x})}} \quad (3)$$

$$\alpha^0(\vec{x}) = -\alpha^1(\vec{x}) - \frac{1}{2} \left(\frac{\nabla \rho^0}{\rho^0} \right)^2 \quad (4)$$

$$F_{q0}(\vec{x}, \omega) = \frac{f_1^0 g(\omega)}{\sqrt{\rho^0}} \left(\delta^2(\vec{x} - \vec{x}_s) - \frac{\nabla \rho^0}{4\pi \rho^0} \cdot \frac{\vec{x} - \vec{x}_s}{|\vec{x} - \vec{x}_s|^3} \right) \quad (5)$$

$$F_{q1}(\vec{x}, \omega) = \frac{f_1^1 g(\omega)}{\sqrt{\rho^0}} \delta(\vec{x} - \vec{x}_s) \delta(z - z_s) \quad (6)$$

F_{q0} and F_{q1} are the source functions corresponding to the impulsive function f of the Cauchy equations. F_{q0} and F_{q1} result after the expansion of $f = f_1^0 + \epsilon f_1^1$.

f_1^0 and f_1^1 accounts for the impulse intensity of the sources that ignites the wave propagation. The function $g(\omega)$ is the Fourier transformation of a source function. In this work, for simplicity purposes, we use a Ricker's function

$$g(\omega) = \frac{\omega^2}{\sqrt{8\pi^3} \omega_d^3} \exp\left(-\frac{\omega^2}{4\pi^2 \omega_d^2}\right) \quad (7)$$

to simulate seismic sources. ω_d is the reference frequency of the sources and for this work we chose $\omega_d = 30\text{Hz}$. At all times we refer herein to ω as the angular frequency $\omega = 2\pi f$, which is measured in $\omega [=]\text{rad/s}$. For simplification, we will express ω in Hz only. For example, $\omega = 40\text{Hz}$ means $\omega = 40\text{rad/s}$.

THE DENSITY FUNCTION $\rho^0(\vec{x})$

As this research is based on the description of waves propagating in a medium with variable density, the Equations 3 - 6 enable forward modelling by using an arbitrary density function. On the other hand, in different contexts, it is more common to work with velocity instead of a density field. A relationship between the density and velocity profiles may be established and, therefore, every equation presented herein could be expressed as a function of a velocity parameter. For example, for some purposes, in geology the density can be expressed as a polynomial of degree 5 in velocity parameter, see [8] : $\rho^0(z, x) = \sum_{i=1}^5 m_i c(z, x)^i$, where m_i are constants.

The formulation presented allows for modelling wave propagation in an arbitrary velocity profile, if a relation between density and velocity is established, by following the recipe: With the velocity profile, it is possible to build a density. Then, by finding the Laplacian and the gradient numerically (of the density map), the maps of $\alpha^0(\vec{x})$ and $\alpha^1(\vec{x})$ from the Equation 3 - 4 can be computed. From this point on, all Equations 3 - 6 would be expressed in terms of velocity. Thus, our formulation allows to express every result in terms of velocity, if so wished.

One of the goals of this research is to explore, in the simplest possible way, the effect of the pseudo-wave vector k^i in the wave propagation with variable density. For such purpose, we will use the density and velocity ratio that is mathematically consistent with the fact that α^0 and α^1 are constants. Hence, we also simplify the

computational analysis, as in this work we make a first approximation to the incident wave by using a perturbative integral modelling.

Then, in order to simplify our modeling, the density profile $\rho^0(\vec{x})$ will be fixed by setting up $\alpha^0(\vec{x})$ and $\alpha^1(\vec{x})$ as constants in the Equations 3 - 4. Let's say $\alpha^0(\vec{x}) = \text{const}_0$ and $\alpha^1(\vec{x}) = \text{const}_1$.

We are interested in exploring deviations of the classical wave vector $k(\vec{x}, \omega) = \omega^2/c^2(\vec{x})$. We will model such minor deviations by adding constant terms, through alpha factors, thus: $k^i(\vec{x}, \omega) = \omega^2/c^2(\vec{x}) + \alpha^i$, for $i=0,1$. Following [7], we choose $\alpha^0 = -b^2/c_0^2$ and $\alpha^1 = +b^2/c_0^2$. The constant c_0 will be explained shortly. With such a choice of the Equations 3 - 4, after some algebra, these are written as:

$$\alpha^1 = \frac{\nabla^2 \rho^0(z, x)}{2 \rho^0(z, x)} - \frac{1}{4} \left(\frac{\nabla \rho^0(z, x)}{\rho^0(z, x)} \right)^2 = + \frac{b^2}{c_0^2} \quad (3a)$$

$$\alpha^0 = \frac{\nabla^2 \rho^0(z, x)}{2 \rho^0(z, x)} - \frac{3}{4} \left(\frac{\nabla \rho^0(z, x)}{\rho^0(z, x)} \right)^2 = - \frac{b^2}{c_0^2} \quad (4a)$$

A density function that satisfies simultaneously the e Equations 3a and 4a and that varies only with depth, is given by

$$\rho^0(z) = \rho_{\text{const}} \text{Exp} \left[\frac{4b}{c_0} (1 + z) \right] \quad (8)$$

where ρ_{const} is a quantity showing density units; however, in the simulations shown here under, this quantity is irrelevant in all equations for the pressure field, as it is algebraically canceled in the expressions. Equation 8 is the relation that we use in this work for modeling of the wave propagation. A general form of the density profile that satisfies simultaneously the Equations 3a - 4a, for arbitrary constants $\alpha^0(\vec{x}) = \text{const}_0$, $\alpha^1(\vec{x}) = \text{const}_1$, can be expressed as

$$\rho^0(\vec{x}) = \rho_{\text{const}} \text{Exp}[\pm \vec{\gamma} \cdot (z, x)] \quad (9)$$

where $\vec{\gamma}$ is any constant vector with the only restriction that $\gamma^2 = |\alpha^0| = |\alpha^1|$. For simplicity, we choose $\rho^0(z)$ in Equation 8, as this work is intended to do a first approximation to the modelling in order to explore integral solutions.

Note that in this approach b is merely a constant that is restricted to obey $\alpha^0 = \text{const}_0$, $\alpha^1 = \text{const}_1$, and, therefore, b can be expressed in several ways in order to explore the perturbative method proposed. For example, parameter b can be expanded as a sum of powers of velocity c_0 : $b = \sum_{l=0}^L a_l c_0^l$, where L , and a_l must be calibrated to have the correct units in the expression for the pseudo-vector $k^i(\vec{x}, \omega) = (\omega^2/(c^2(\vec{x})) + \alpha^i)$, for $i=0,1$.

In this work, we consider b a constant and it is compared with the frequency, i.e., $L=0$, and $a_0 = \omega$.

On the other hand, parameter b can be complex, and can be related to the quality factor Q [9], linked to the attenuation or dispersion effects; for example, the expression (4a) opens the door for consideration of such cases.

CONTRAST VELOCITY $C(\vec{x})$, THE VELOCITY C_0 , AND THE SOLUTION OF THE WAVE EQUATION

The quantity c_0 appearing in Equation 8 is the wave velocity in the medium from where the wave is coming. $c(\vec{x})$ represents the wave

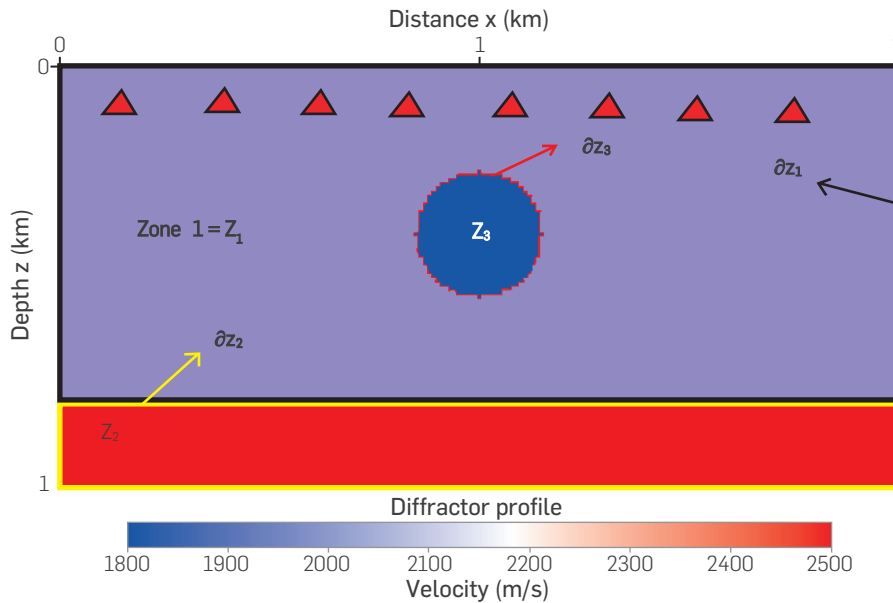


Figure 1. The zones, boundaries Z_i , and the wave velocity c_0 concepts are illustrated.

velocity of the medium to which the wave is entering, thus the difference between $c(\vec{x})$ and c_0 will be that the former is the velocity of the “refracting zone”, while the latter is the wave velocity in the medium of incidence. It should be stressed that c_0 does not represent the background velocity of the whole subsurface.

We used a classical solution strategy of the Helmholtz equation with constant wave-vector k^i , for $i=0,1$, in order to approach a numerical solution for (2), see [10]–[11]. As we are interested in wave propagation in media with variable density, it is essential to describe the sense in which such classical solution of Equation 2 is used. We define and illustrate the concept of the zone with the aim of explaining how we used the solution of the Helmholtz equation with constant wave vector.

Figure 1 shows the concept of the zones Z_i in the medium. This figure is included for illustrative purposes only, and it is used just to clarify the concepts of zone and the boundary of a zone. In the particular situation of Figure 1, the sources are disposed near the surface; however, their position can vary for other experiments. Energy sources are symbolized as red triangles close to the surface. The medium of Figure 1 is made up of a first layer: $z \in (0, 0.75)$ km with wave velocity of 2000 m/s, the second layer: $z \in (0.75, 1)$ km with wave velocity of 2500 m/s, and a circular diffractor with wave velocity of 1800 m/s.

When a source is ignited, the wave propagates from Z_1 to Z_3 . Z_1 is the medium from which the wave will strike the contrast medium Z_3 ; therefore, the wave velocity (The velocity values can be changed for use in other applications such as medical imaging), is taken as $c_0 = 2000$ m/s; for this layer $k^i(\vec{x}, \omega) = \omega^2 / 2000^2 + \alpha^i$. In this case, the contrast medium has a wave velocity of $c(\vec{x}) = 1800$ m/s.

Likewise, when the wave crosses the boundary ∂Z_3 (red line), going from Z_3 to Z_1 , Z_3 is the medium from where the wave will strike the contrast zone Z_1 . In this case, with the wave going from Z_3 to Z_1 , the wave velocity c_0 is equal to 1800 m/s; $c(\vec{x}) = 2000$ m/s, and $k^i(\vec{x}, \omega) = \omega^2 / 1800^2 + \alpha^i$.

Finally, when the wave crosses ∂Z_2 (yellow line), going through from Z_1 to Z_2 , the corresponding c_0 wave velocity is 2000 m/s and $c(\vec{x}) = 2500$ m/s. Therefore, for each boundary inside the medium an incident wave, with velocity c_0 , must be calculated. The following considerations are to be borne in mind to solve Equation 2 presented herein:

- **Boundary conditions.** The partial differential Equation 2 has a family of infinite solutions, and a particular solution must be chosen for implementing numerical solutions. The difference between each solution is given by the boundary conditions of the surface in which the specific problem is to be solved. Different solutions, or different boundary conditions, are shown and explained in [10]–[11]. We have chosen the half plane as surface to solve Equation 2, as it is natural in the seismic problem.

The Boundary conditions used are those for the half plane defined by $\{(x, z) | x \in \mathbb{R}, z \in \mathbb{R}^+\}$, with the depth denoted by z , and horizontal extension along the x -axis by x . This means that the solution to Equation 2, implemented herein, is for a half plane only and, therefore, a reflection, on the surface $z = 0$ km, will appear in all simulations of this work. Another consequence of this solution in a half plane is that the incident wave, over the boundaries of all zones inside the medium, will contain the natural reflection in the boundary at the surface $z = 0$ km. The reflection at the surface $z = 0$ km is considered a reflection in the background; therefore, all the incident waves will contain the reflection of the background, coming from the boundary at $z = 0$ km, and imposed by the solution of the half plane.

- The half plane is considered a wall, consisting of different non-regular zones. Those zones represent the different materials conforming that wall. For example, in geophysics those zones are all types of rocks, basalts, sands, clays, etc.

Those irregular zones will be denoted by Z_i and its boundaries by ∂Z_i . The boundaries ∂Z_i play the role of the boundary between one material, for example a rock, and other material, for example basalt.

- Inside one zone Z_i , juxtaposed to a zone Z_i' any function is supposed to be differentiable and smooth. It must be noted that the wave vector, $k^i(\vec{x}(z_i), \omega)$, is taken as a constant inside a fixed zone Z_i . Just at the boundaries ∂Z_i all the functions are not required to be differentiable.

The solution of the Helmholtz equation used here (see [10], [11]) with constant wave-vector is valid inside every Z_i . Although boundary conditions must be imposed on each ∂Z_i to match solutions between every pair of zones Z_i – Z_i' , we will ignore this matching in order to find an approximation to the incident field for each zone Z_i of a medium. Approximations for the reflected or transmitted fields are left for future work.

The approximation of constant zone or Born approximation can be seen as a method to calculate the incident wave in the Neumann's series solution of the Helmholtz equation [12]; i.e., the Equation 2 can be expressed, after a bit of algebra, as:

$$(\nabla^2 + \frac{\omega^2}{c_0^2} + \alpha^j) q^j(\vec{x}, \omega) = F_{q^j}(\vec{x}, \omega) - \left[\frac{\omega^2}{c^2(\vec{x})} - \frac{\omega^2}{c_0^2} \right] q^j(\vec{x}, \omega) \quad (10)$$

where the source term $F_{q^j}(\vec{x}, \omega)$ accounts for the incident wave (Incident wave is incident to each boundary) and the term in the square parenthesis is called the contrast term,

$$\chi(\vec{x}, \omega) = \frac{\omega^2}{c^2(\vec{x})} - \frac{\omega^2}{c_0^2}$$

where c_0 is the wave velocity of the medium from which the wave will strike, as it was illustrated in the discussion of Figure 1.

The contrast term has been introduced by [13] and [14] in the context of the Contrast Source Inversion (CSI) method. $\chi(\vec{x}, \omega)$ has been recently used in medical applications [15]-[16]. The $\chi(\vec{x}, \omega)$ term can be a good choice for wavefield inversion in seismic exploration, since iterative inversion methods, like FWI [17]-[18], use schemes that start with a guess of the velocity profile, which is updated at each step of the method. The pressure field is calculated from such assumed velocity profiles, and thus the velocity profile is known for every iteration of the whole inversion process.

Equation 10 constitutes a nonlinear problem, since $\chi(\vec{x}, \omega)$ is an unknown, and its solution can be expressed, by using $\vec{x}=(z, x)$, as a Fredholm [19] integral equation like

$$q^j(x, z, \omega) = q_{inc}^j(x, z, \omega) + q_{sct}^j(x, z, \omega) \quad (11)$$

where $q_{inc}^j(x, z, \omega)$ is the incident wave that satisfies,

$$q_{inc}^j(x, z, \omega) = -\int_{-\infty}^{\infty} \int_0^{\infty} G(x, x', z, z', \omega) F_{q^j}(x', z') dx' dz' \quad (12)$$

and $q_{sct}^j(x, z, \omega)$ is the scattered contribution to pressure field given by

$$q_{sct}^j(x, z, \omega) = \int_{-\infty}^{\infty} \int_0^{\infty} G(x, x', z, z', \omega) \chi^j(x', z', \omega) q^j(x', z', \omega) dx' dz' \quad (13)$$

The propagator $G(x, x', z, z', \omega)$, is the solution of the wave equation for a point source

$$(\nabla^2 + k_0^j(\omega)) G(x, x', z, z', \omega) = \delta(x - x') \delta(z - z')$$

where $k_0^j(\omega) = \omega^2/c_0^2 + \alpha_0^j$.

A solution of such Fredholm integral Equation 13, can be approximated through the Born approximation [19], for which

$$q^j(x, z, \omega) = q_{inc}^j + \int_{-\infty}^{\infty} \int_0^{\infty} G(x, x', z, z', \omega) \chi^j(x', z', \omega) q_{inc}^j(x', z', \omega) dx' dz' \quad (14)$$

Such Born approximation can be considered a member of an iterative solution often called Neumann series, for which (14) is taken as the first term (i.e., $q^j(x, z, \omega) = q^{j(1)}(x, z, \omega)$) and the second term is calculated as

$$q^{j(2)}(x, z, \omega) = q_{inc}^j + \int_{-\infty}^{\infty} \int_0^{\infty} G(x, x', z, z', \omega) \chi^j(x', z', \omega) q^{j(1)}(x', z', \omega) dx' dz' \quad (15)$$

The set of the resulting values $\{q^{j(1)}, q^{j(2)}, q^{j(3)}, \dots\}$ conforms the Neumann series ([12], page 578, equation 9.336). For arbitrary contrasts and arbitrary density profiles, this series does not converge. The number of terms that must be included in the series depends on the particular problem but all the process rests on the possibility to compute the incident term, q_{inc}^j . Since this research is devoted to compute incident waves, from this point on, carrying the subscript "inc" might become redundant. From now on, we are focused in computing $P_{inc}^j = \sqrt{\rho^0} q_{inc}^j = 0, 1$. To simplify it, we will remove the subscript "inc".

Thus, the Equation 2 can be solved [10], by using the relation $q^j = P^j / \sqrt{(\rho^0)}$, in two dimensions and for the boundary condition of the half plane explained above, as

$$P^i(x, z, \omega) = \sqrt{\rho^0(z)} \int_{S'} F_{q^i}(x, z, \omega) G(x, x', z', z, \omega) dS' \quad (16)$$

where S' is the boundary of the entire half plane and the Green's function depends on whether k^i is complex or real. The functions $F_{q^i}(x, z, \omega)$, $i=0, 1$, are the Fourier transforms in time of the sources, given in the Equations 5 and 6.

3. EXPERIMENTAL DEVELOPMENT

Our main solution is written in equation (16); however, there are two cases to be considered: (1) A case for complex wave vector k^i , which means a regime of high dispersion, i.e., $\omega < b$. (2) A case for real wave vector k^i associated with low dispersion, i.e., $\omega > b$. The case $b = \omega$ is not related to deviations of the wave vector and, therefore, it is left out. Next, we study each case individually.

COMPLEX WAVE VECTOR k^i : $\omega < b$

In order to facilitate the reading of equations let us remember the notation introduced so far: the position vector is $\vec{x}=(x, z)$, the positions of the sources are $\vec{x}_s=(x_s, z_s)$, the differential elements in the integral symbols is $d\vec{x}=dx dz$, the intensity of impulse force up to zeroth and first order are f_i , $i=0, 1$, and the variable density up to zeroth order is $\rho^0(\vec{x})$.

Let us define auxiliary variables

$$\Omega^+ = \frac{\omega^2 - b^2}{c_0^2}, \quad \Omega^- = -\Omega^+, \quad a_1 = \sqrt{\Omega^-} r_1, \quad a_2 = \sqrt{\Omega^-} r_2,$$

$$r_1 = \sqrt{(x-x')^2 + (z-z')^2}, \quad r_2 = \sqrt{(x-x')^2 + (z+z')^2},$$

$$b_1 = \sqrt{\Omega^+} r_1, \quad b_2 = \sqrt{\Omega^+} r_2.$$

On this basis, according to [10], the pressure field is written in terms of modified Bessel functions of the second kind and zeroth order, denoted by K_0 . The argument of K_0 involves the wave vector k^i and c_0 , through Ω^\pm , a_1 or a_2 . K_0 is complex and, therefore, the final expressions for P^i are real, and given by:

$$P^0(\vec{x}, \omega) = \sqrt{\frac{\rho^0(\vec{x})}{\rho^0(\vec{x}_s)}} \frac{f_l^0 g(\omega)}{2\pi} [K_0(\sqrt{\Omega^-} |\vec{x} - \vec{x}_s|) - K_0(\sqrt{\Omega^-} \sqrt{(x - x_s)^2 + (z + z_s)^2})] - \frac{f_l^0 g(\omega) \sqrt{\rho^0(\vec{x})}}{8\pi^2} \quad (17)$$

$$P^1(\vec{x}, \omega) = - \sqrt{\frac{\rho^0(\vec{x})}{\rho^0(\vec{x}_s)}} \frac{f_l^1 g(\omega)}{2\pi} [K_0(\sqrt{\Omega^-} |\vec{x} - \vec{x}_s|) - K_0(\sqrt{\Omega^-} \sqrt{(x - x_s)^2 + (z + z_s)^2})] \quad (18)$$

Note that P^1 has not an integral part because F_{q1} in (5) contains only one term, while F_{q0} has two terms.

REAL WAVE VECTOR k : $\omega > b$

In this case, the pressure is complex and is given by [10]

$$P^0(\vec{x}, \omega) = i \sqrt{\frac{\rho^0(\vec{x})}{\rho^2(\vec{x}_s)}} \frac{f_l^0 g(\omega)}{4} [H_0^2(\sqrt{\Omega^+} |\vec{x} - \vec{x}_s|) - H_0^2(\sqrt{\Omega^+} \sqrt{(x - x_s)^2 + (z + z_s)^2})] - i \frac{f_l^0 g(\omega) \sqrt{\rho^0(\vec{x})}}{16\pi} \int_0^\infty \int_{-\infty}^\infty \frac{(\vec{x}' - \vec{x}_s)}{|\vec{x}' - \vec{x}_s|^3} \cdot \frac{\nabla \rho^0(\vec{x}')}{\rho^{03/2}(\vec{x}')} [H_0^2(b_1) - H_0^2(b_2)] d\vec{x}' \quad (19)$$

$$P^1(\vec{x}, \omega) = -i \sqrt{\frac{\rho^0(\vec{x})}{\rho^2(\vec{x}_s)}} \frac{f_l^1 g(\omega)}{2} [H_0^2(\sqrt{\Omega^+} |\vec{x} - \vec{x}_s|) - H_0^2(\sqrt{\Omega^+} \sqrt{(x - x_s)^2 + (z + z_s)^2})] \quad (20)$$

where $H_0^2 = J_0 - iY_0$ is the Hankel function of the second kind and zeroth order. These (x, z) are the coordinates denoting the position in which we are evaluating the pressures P^i in a specific zone, and (x', z') denote the points for all half planes.

The solutions (17), (18), (19), and (20) implicitly depend on c_0 through ρ^0 and Ω^\pm . As discussed above, c_0 represents a constant wave velocity in a specific zone Z_i and thus c_0 is a constant for the integrals in equations (17) and (19). The equation (8) is needed in the integrals (17) and (19). Note that the integral parts differ from zero for variable density profiles only.

We have nicknamed Integral Solutions (IS) to the set of equations (17)–(20) plus a representation of density, for example as (8). The equations (17) and (19) will be named integral part of the IS and we cite it as IP. The part of the IS not containing integral expression, (18) and (20), will be named as functional part and symbolized by FP.

Computational implementation of IS was made by using a rectangular grid of horizontal extension $L_x = 1000\text{m}$, vertical extension $L_z = 1000\text{m}$. The mesh was discretized with $N_x = 1000$, points along x-axis, $N_z = 1000$ points along z-axis, and, therefore, distance between points are $\Delta x = \Delta z = 1\text{m}$. In most cases, the source was disposed at $(x_s, z_s) = (500, 500)\text{m}$. The reference frequency of Ricker's function, $g(\omega)$, was $\omega_0 = 30\text{Hz}$.

The set of frequencies $\omega = 5\text{Hz}, 10\text{Hz}, 20\text{Hz}, 30\text{Hz}, \dots, 140\text{Hz}$ was used to run the modeling. The scalar intensities f_l^i of equations (17)–(20) were fixed to the unit. The perturbative parameter of expansion was chosen as $\epsilon = 0.1$.

The computational implementation and its analysis of the case $\omega > b$ is presented hereunder. Results of implementation for the case $\omega < b$ were similar to the former and added no new elements to the discussion. Therefore, they are not included herein.

The integrals have been implemented by using free routines (GSL-GNU Scientific libraries), specially the Monte-Carlo integration technique. A parallelized implementation with MPI was employed to calculate the integral over the full grid. Since the integrals (17) and (19) have oscillatory terms, a VEGAS algorithm was used to avoid the problems introduced by the oscillatory behavior of the integrand. VEGAS approximates the distribution by following a number of steps over the integration region while histogramming the function integrand. Each histogram is used to build the sampling distribution for the next step. Three computational experiments are presented in the field of exploration seismic.

4. RESULTS ANALYSIS

Three computational experiments are presented, which can be fitted in the context of exploration seismic. These experiments consist on the propagation of waves in three different media: the first experiment consists of a medium with constant velocity, the second one consists in 3 layers with velocities $c_1 < c_2 < c_3$, and the last one containing complex velocity profiles and having sharp peaks.

FIRST EXPERIMENT: CONSTANT VELOCITY, VERIFICATION OF CORRESPONDENCE PRINCIPLE

We first analyzed a medium with one layer of constant velocity to explore how our implementation reproduces simple wave propagation. Often this procedure is called verification of the correspondence principle. The functional part (FP) of the integral solution (IS) was modeled inside a medium with a uniform velocity of $c = 3000\text{m/s}$.

Pressure field of propagating waves in a medium with velocity $c_0 = 3000\text{m/s}$ and with frequencies of 5Hz and 100Hz are displayed in **Figure 2**. The color map represents the intensity of the real part of the pressure, measured in Pa. For this experiment, the source is placed at the center $(x_s, z_s) = (500, 500)\text{m}$; note that this position differs from the sources shown in **Figure 1**.

Note the symmetry with respect to line $x = 500\text{m}$, which is expected. The solution include the boundary conditions of a half plane for $z = 0\text{m}$ and the wave that moves upwards from the center (x_s, z_s) is reflected at the line $z = 0\text{m}$. Due to the boundary condition at $z = 0\text{m}$ it is possible to observe an asymmetry with respect to $z = 500\text{m}$,

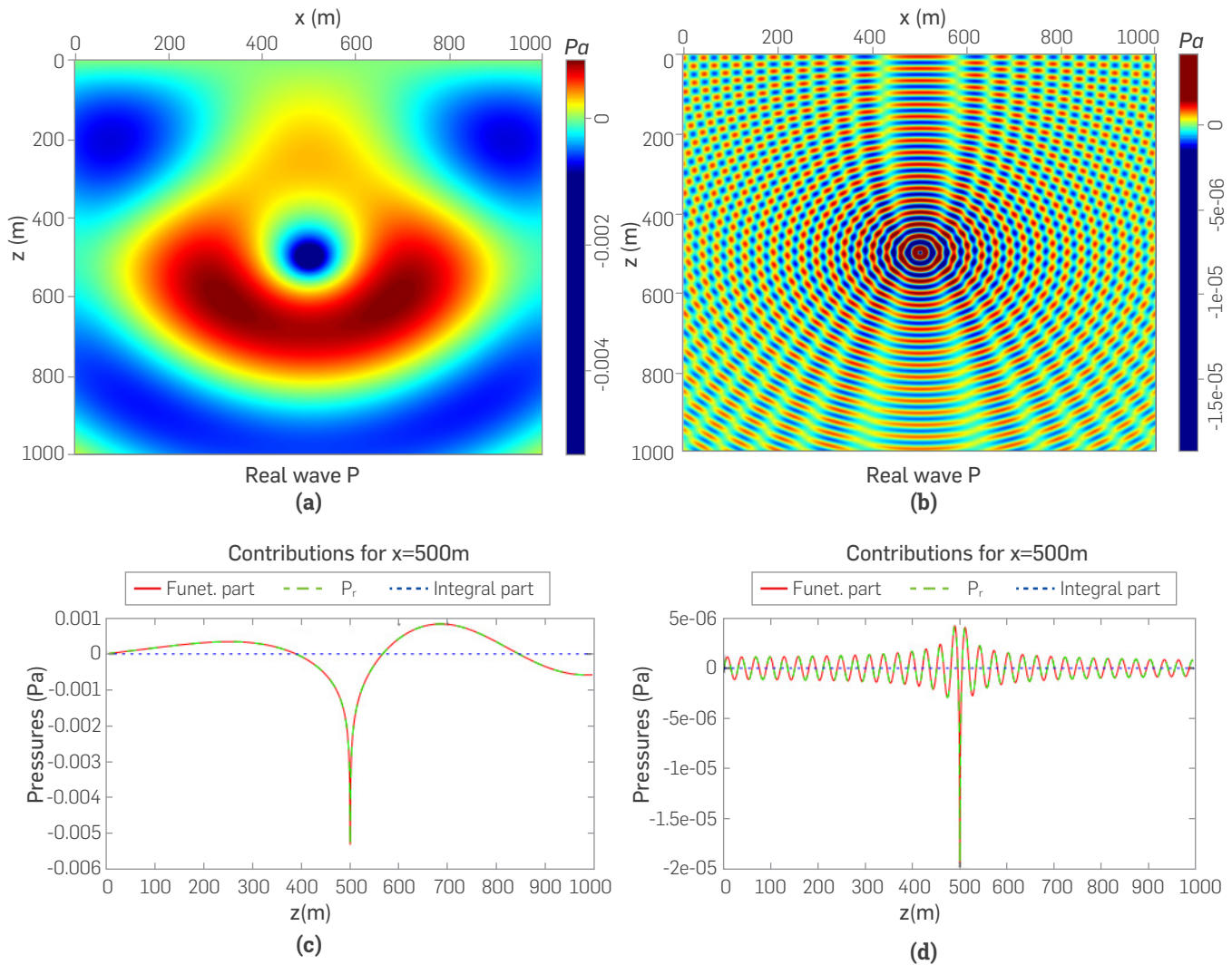


Figure 2. Demonstration of waves propagating inside a medium with uniform velocity $c_0=3000\text{m/s}$. The pressure is given in Pa and coordinates are measured in m. The left column (Figure 2a and 2c) displays waves with 5Hz, this is why the wave length $\lambda=600\text{m}$, and the right column (Figure 2b and 2d) corresponds to 100Hz. Figures (a) and (b) show patterns of interference because of the reflection at $z=0\text{km}$.

as it is shown in **Figures 2c – 2d** for the real part. For $\omega=5\text{Hz}$ the wave length is $\lambda=600\text{m}$; therefore, in the second half of the plane, $z>500\text{m}$, only $5\lambda/6$ is observed. An analogous behavior is observed for the imaginary part and, therefore, it is not shown.

In **Figures 3a and 3b** we show the IP of the field and it is possible to observe the low magnitudes of IP with respect to FP. $\text{IP}\sim 10^{-12}\text{Pa}$ for 5Hz and $\text{IP}\sim 10^{-14}\text{Pa}$ for 100Hz, compared with its corresponding $\text{FP}\sim 10^{-3}\text{Pa}$ and $\text{FP}\sim 10^{-6}\text{Pa}$, respectively. This shows clearly that with respect to a uniform medium, the contribution of the IP can be ignored safely in a first approximation, as the IP values have magnitudes comparable with the numerical noise.

SECOND EXPERIMENT: THREE LAYERS

In this experiment we used a velocity profile with three layers M_1 , M_2 and M_3 , consisting of $c_1=2000\text{m/s}$, $c_2=3000\text{m/s}$ and $c_3=4000\text{m/s}$

at depths $M_1=(0,200)\text{m}$, $M_2=(200,800)\text{m}$ and $M_3=(800,1000)\text{m}$ respectively.

The purpose of this configuration is to explore how the IS models the changes from one layer to another; those interfaces are traditionally referred to, in the inverse theory, as reflectors. **Figure 4** shows the results for the parameters frequency and dispersion: $(\omega, b)=(5, 0)\text{Hz}$.

It must be noted that changes in speed, for each layer, introduce changes in wavelength λ . Thus, inside M_1 , $\lambda_1=400\text{m}$ and thereupon the wave reaches half an oscillation in the first layer. The same occurs in medium M_2 , in which the wave has a wavelength $\lambda_2=600\text{m}$ and, since the spherical pulse starts at $(x_s, z_s)=(500, 500)\text{m}$, the perturbation only completes half oscillation. In the last piece of travel M_3 , the wave performs only a quarter of one oscillation inasmuch as its wavelength is $\lambda_3=800\text{m}$.

The interfaces, at 200m and 800m, can be clearly observed in the modelling results, as it is illustrated in **Figures 4**. It is visible in

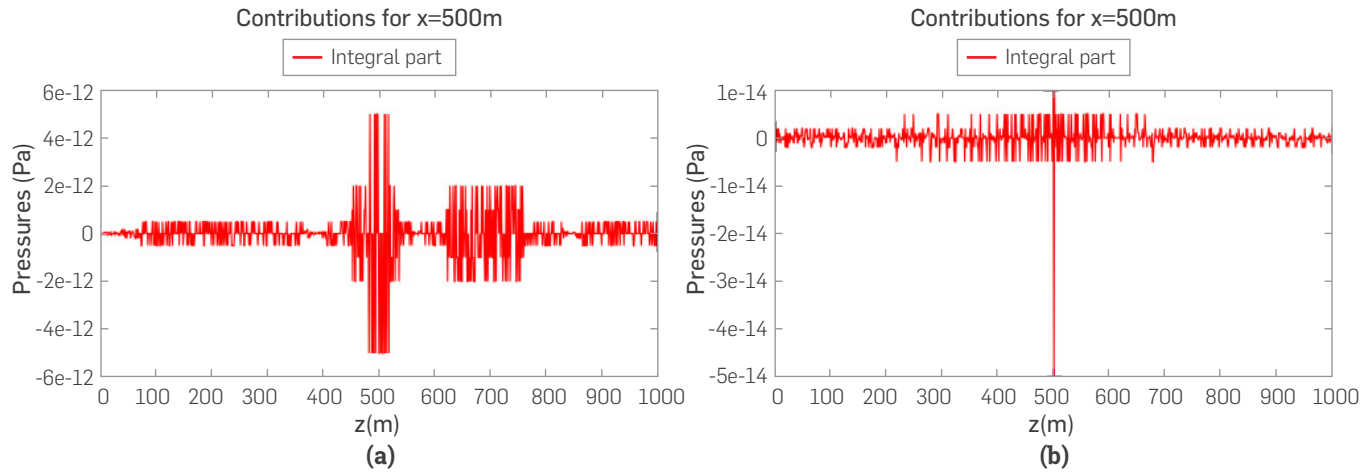


Figure 3. The integral part IP for a constant velocity profile along x=500m. It must be noted that magnitudes are IP $\sim 10^{-12}$ Pa or IP $\sim 10^{-14}$ Pa, for 5Hz (a), and for 100Hz (b), respectively.

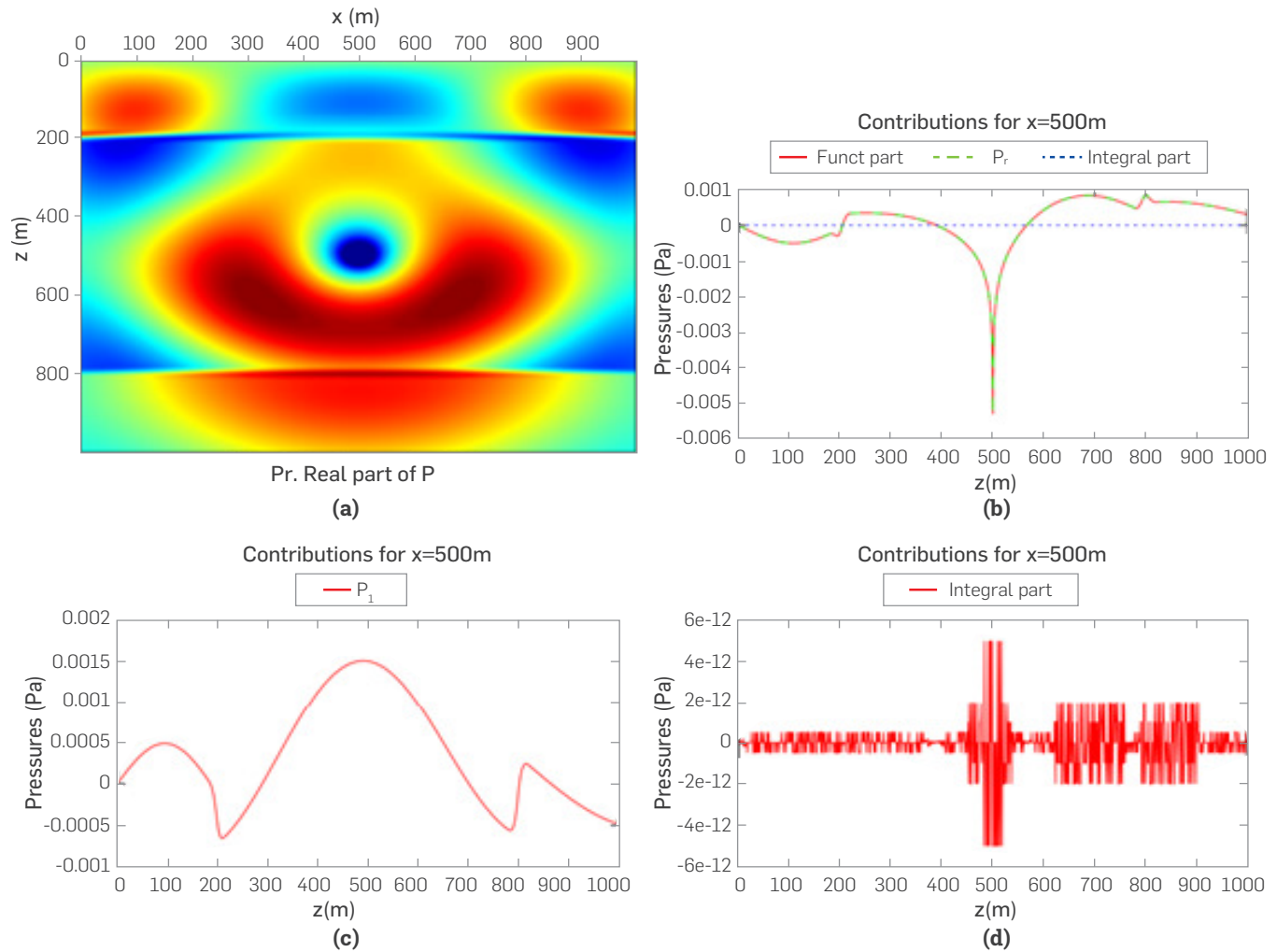


Figure 4. These pictures show the modelling in a 3-layer medium. For this simulation $(\omega, b) = (5, 0)$ Hz. (a) The propagation from center of the half plane, the three layers are well delineated. (b) The real part of the IP, P_r , and total pressure P_t are shown. (c) The imaginary part of field P_i . (d) The integral part, IP, is shown. The small contribution of the IP can be observed in all of figures.

Figure 4b, for $z=200\text{m}$; the pressure therein changes sign, when the energy goes from M_2 to M_1 . However, for $z=800\text{m}$, it can be observed that there is not a flip of sign in the transmitted wave to the zone of 4000ms^{-1} . In **Figure 4c**, we show the imaginary part, P_{im} , of the pressure field for the shot displayed in **Figure 4a**, in order to provide a verification that irregular behavior does not happen in the imaginary component of IS; for P_{im} , only changes in amplitude are observed, just in the interfaces at 200m and 800m .

Figure 4b also suggests that IP does not add anything to the magnitude of P . To see this, it was drawn in **Figure 4d** where the IP is drawn as a function of depth z . The largest amplitude of the IP is around 4×10^{-12} Pa, nearly 10^9 times smaller than its FP.

THIRD EXPERIMENT: STRONG CONTRASTS

To examine the behavior of the IS in a complex medium, with many sharp edges and strong lateral changes of density (velocity), like Marmousi, we first generate propagations in a simple and unrealistic velocity model, as that shown in **Figure 5a**.

The yellow zone corresponds to 2000m/s , the orange zone to 5000m/s , the red zone to 8000m/s , the brown zone to 11000m/s . The shot has a frequency of $\omega=100\text{Hz}$ and the source was located at the center of the medium. The wavelengths in each zone are $\lambda_{\text{yellow}}=20\text{m}$, $\lambda_{\text{orange}}=50\text{m}$, $\lambda_{\text{red}}=60\text{m}$, and $\lambda_{\text{brown}}=110\text{m}$. It can be observed in **Figure 5b** that there are changes of wavelength between different velocities in the medium. The changes of direction of the wave-vector at the interfaces are well defined. The reflectors (interfaces) are clearly modeled. Furthermore, the ability of IS to define sharp zones is clearly demonstrated.

FOURTH EXPERIMENT: THE MARMOUSI MODEL

The Marmousi velocity profile is an important profile widely used in the field of seismic inversion to verify how faithful the final image

is, produced by the algorithms applied to a distorted Marmousi. The structural model of Marmousi is based on a profile through the North Quenguela Trough in Angola [20]. It has a complex structure that allows many reflections and transmissions of propagating waves. With this simulation, we demonstrate the behavior of the IS in a complex profile, where the IP remains almost five orders of magnitude below the FP, as it is displayed in the last two plots of **Figures 6**.

Figure 6a shows the real part and complex modulus of the wavefield. The black, pink, red and blue arrows refer to wedges, domes, faults and places with higher velocities, respectively. In **Figure 6b**, the shot is located at the center of the profile. In **Figure 6c** and **6d**, it can be observed that the IP of pressure is always smaller than its FP.

Figure 7 displays the real part and the complex modulus of the pressure field generated by three shots from the surface at positions $z_s=15\text{m}$, $x_s=2000\text{m}$, 4250m , 9000m . It can be observed that the wavefield, for different source locations, outlines different parts of the model.

We performed a detailed convergence analysis showing that the results presented herein are independent of the number of evaluations of the Montecarlo function; however, we do not present such analysis here, see [21]. This exercise also includes an analysis of parameter b whereby it is concluded that the impact of b on the simulations is negligible and is related to the intensity of amplitude therefore, the conclusions of simulations apply.

More simulations, as function of frequency ω , were carried out to analyze the IP of IS, and the same conclusions were obtained. For instance, in **Figure 8**, the results of the imaginary part of the IP, for frequencies 5Hz , 30Hz , 40Hz , and 50Hz ; for $b = 20\text{Hz}$, are exhibited. The IP is 10^5 orders of magnitude smaller than its functional part FP. This fact could be an important factor, because this allows saving much calculating P , i.e. this fact might make it viable to use this kind of solution IS to do modeling without long times of computation. Up to this point we can conclude that the contribution to the pressure

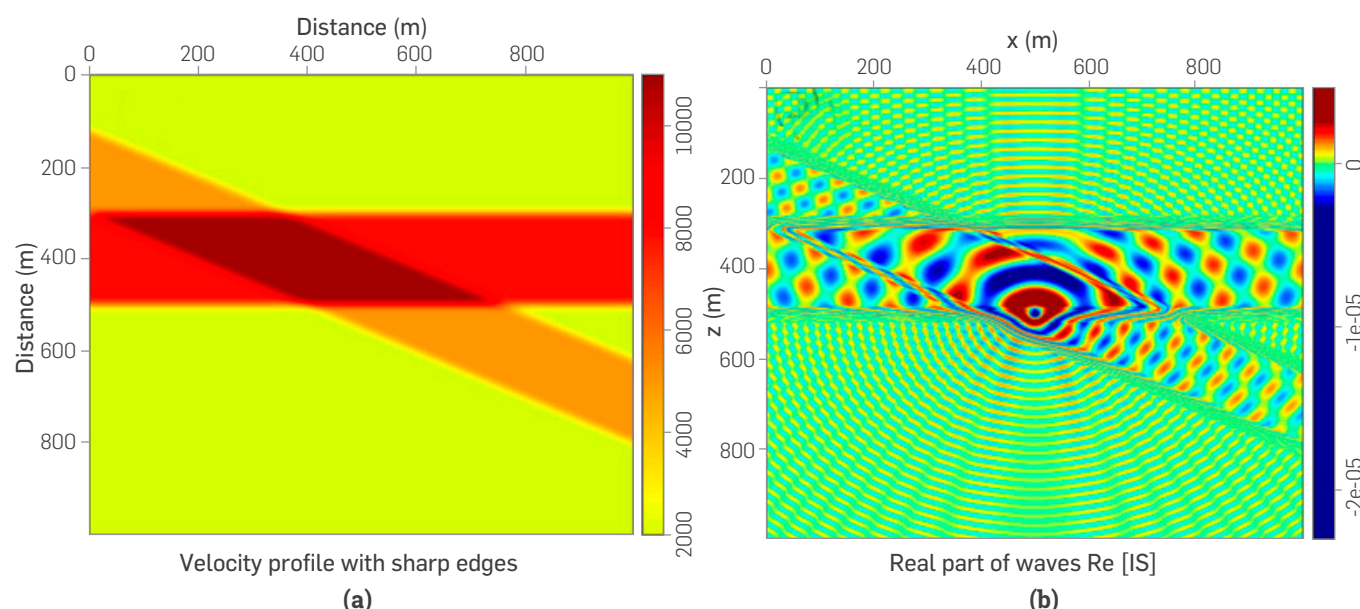


Figure 5. (a) A simple and unrealistic velocity profile with sharp edges allows examining the behavior of the IS for strong lateral changes in density. (b) Propagation of pressure waves from the center through the velocity profile of (a). Note how the interfaces are delineated by the IS, especially the sharp zones.

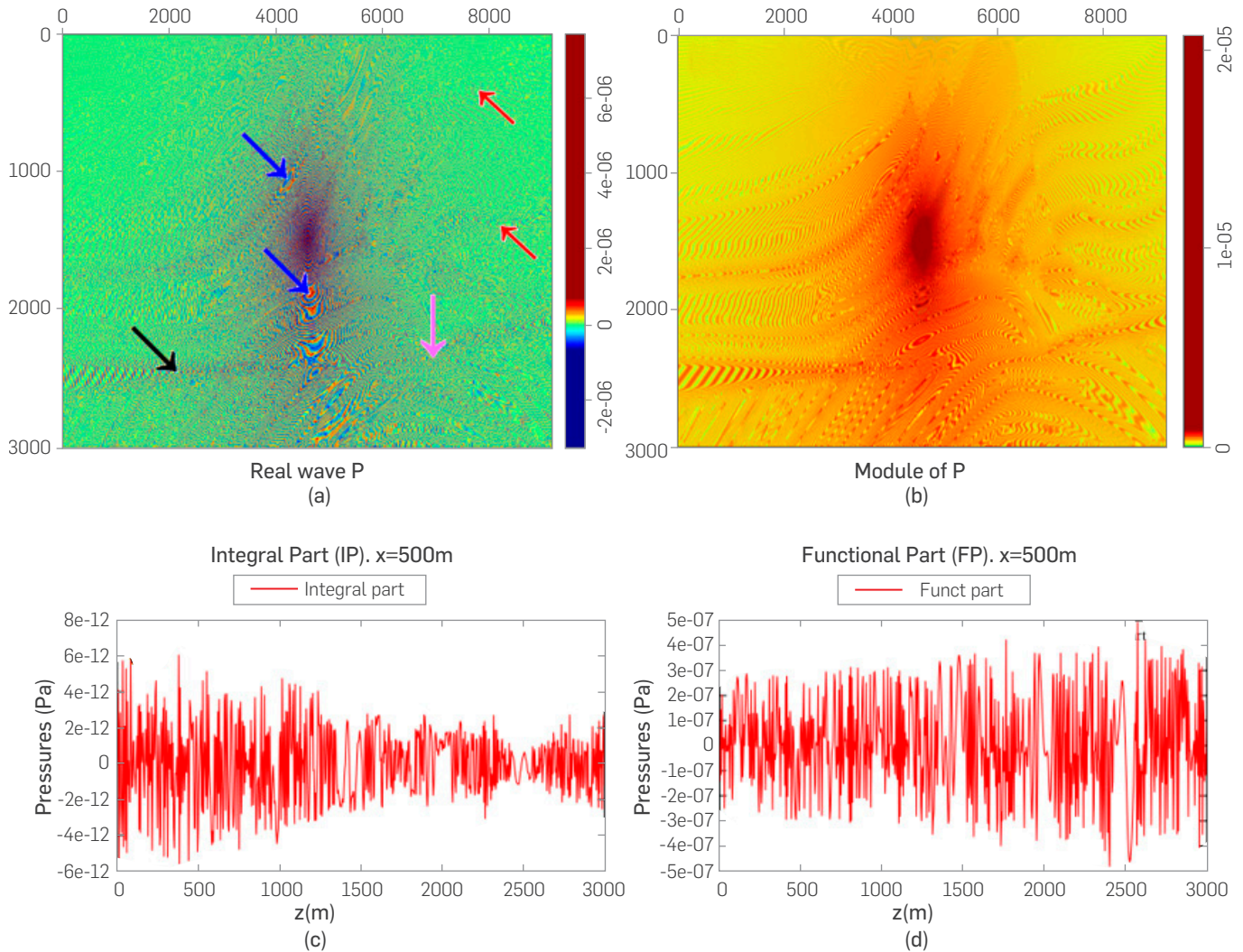


Figure 6. Propagation of a wave with $\omega=100\text{Hz}$ and $b=20\text{Hz}$, from the center through Marmousi. It is used to show how IS delineates the interfaces in the model. (a) The $\text{Re}[\text{IS}]$ is plotted and the level of definition of equation (20) is pointed out by using colored arrows. (b) The complex modulus of (IS) is shown. (c) and (d) show the difference ($\sim 10^5$) between the IP and FP.

of the integral terms IP is sufficiently small to assure that a good approximation of pressure may be made without the IP term. This is the most important result arising from these simulations. This allows modeling pressure by using a simple formula for $P=P^0+\epsilon P^1$

$$P(x, z, \omega) = I(x, z, \omega) \gamma \left[[Y_0(\tilde{k} |r - r_s|) - Y_0(\tilde{k} |r - r_s|^+)] + i[J_0(\tilde{k} |r - r_s|) - J_0(\tilde{k} |r - r_s|^+)] \right] \quad (21)$$

where

$$I(x, z, \omega) = \frac{\sqrt{\rho^0(x, z)}}{\sqrt{\rho^0(x_s, z_s)}} \frac{g(\omega)}{2}, \quad \gamma = (0.5I^0 + \epsilon I^1), \quad \tilde{k} =$$

$$\frac{\sqrt{\omega^2 - b^2}}{c_0}, \quad |r - r_s| = \sqrt{(x - x_s)^2 + (z - z_s)^2}$$

$$\text{and } |r - r_s|^+ = \sqrt{(x - x_s)^2 + (z + z_s)^2}$$

On analogy with Hankel functions, equation (21) can be written as

$$P(x, z, \omega) = I(x, z, \omega) \gamma \bar{H}_0(x, z; \omega) \quad (22)$$

by defining $\bar{H}_0 = \bar{Y}_0 + i\bar{J}_0$, where $\bar{J}_0 = J_0(\tilde{k} |r - r_s|) - J_0(\tilde{k} |r - r_s|^+)$ and similar for \bar{Y}_0 . Equation (22) is an approximated analytic formula to obtain pressure waves propagating inside a variable density medium; it can be used especially for modelling waves inside the earth.

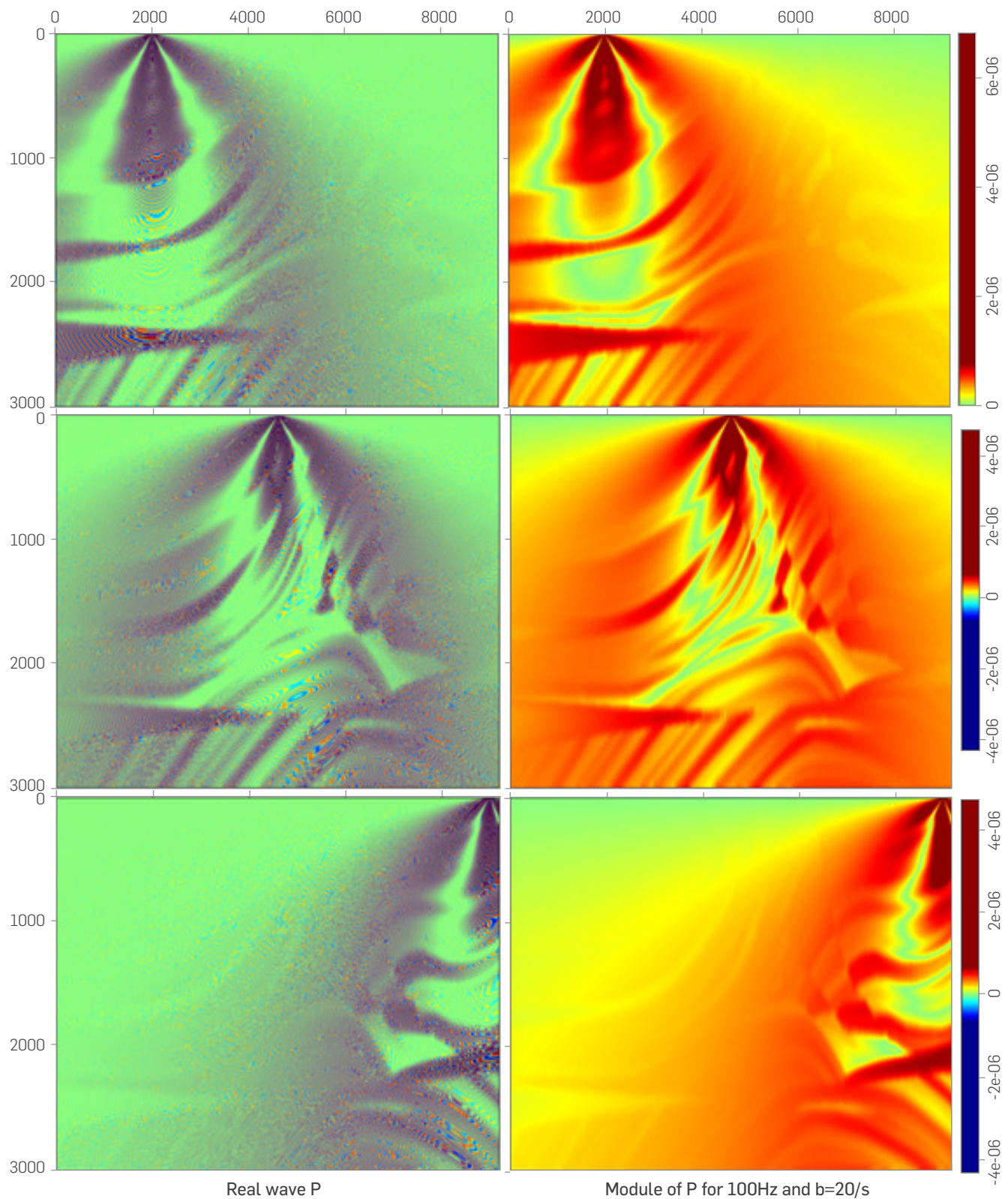


Figure 7. Three shot experiments near the surface in the Marmousi profile. Several positions of the shots are displayed, to illustrate how the interfaces are delineated by the IS. Due to the different positions of the sources, some zones in the model are better delineated than others.

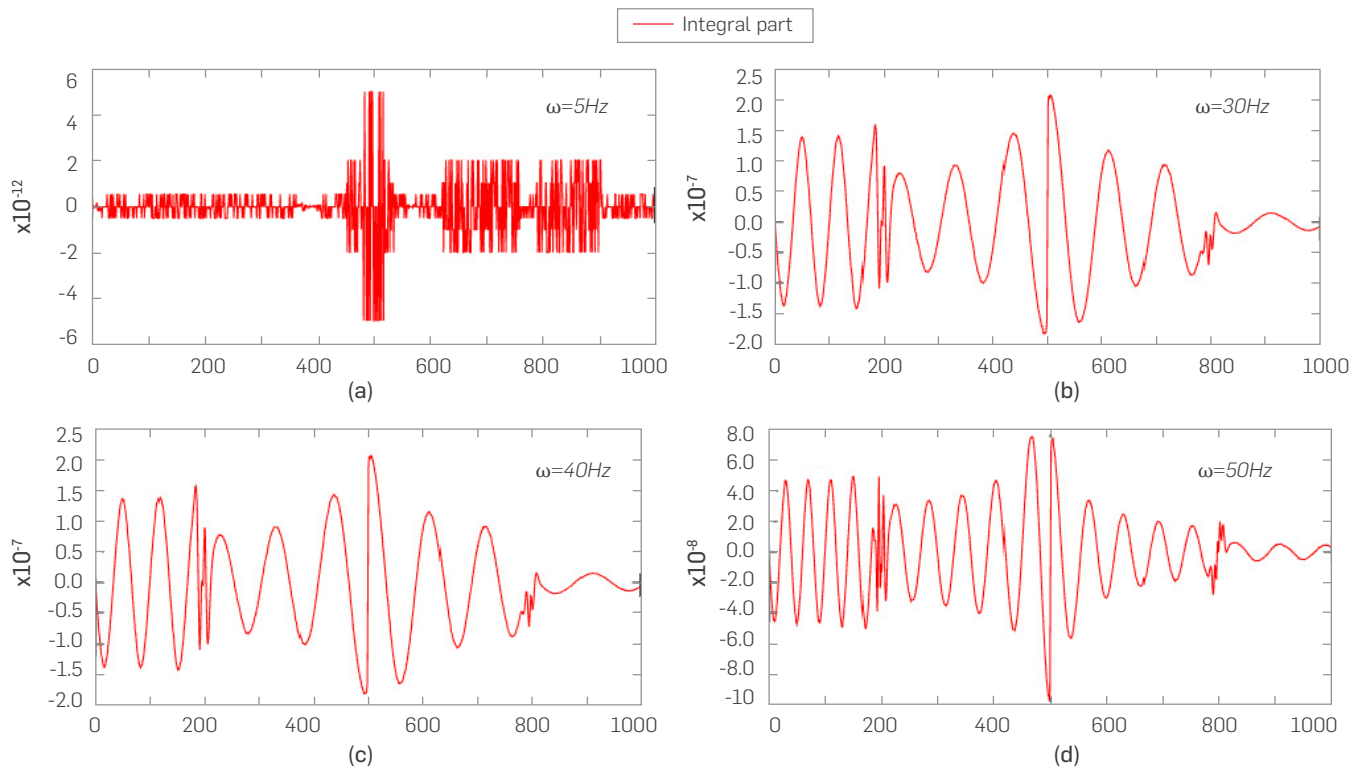
$IP(Pa)$ vs $z(m)$. Contributions for $x=500m$ 

Figure 8. A scanning of the imaginary part of the IP. (a) For $\omega=5\text{Hz}$ $\text{Im}[IP] \sim 10^{-12}\text{Pa}$. (b) For $\omega=30\text{Hz}$ $\text{Im}[IP] \sim 10^{-7}\text{Pa}$. (c) For $\omega=40\text{Hz}$ $\text{Im}[IP] \sim 10^{-7}\text{Pa}$. (d) For $\omega=50\text{Hz}$ $\text{Im}[IP] \sim 10^{-8}\text{Pa}$.

CONCLUSIONS

In this paper we present the basics of a formalism intended to provide an alternative solution to the forward problem in the scenario of seismic inversion. Cauchy's equations for pressure waves propagating inside a medium with a variable density profile were deduced and analyzed. Solutions to Cauchy's equation were presented through a perturbative approach up to first order from which we were able to define an equivalent Helmholtz equation for the propagation of waves in such medium, with variable density.

The Helmholtz equation for the medium with variable density was expressed as a Fredholm integral equation, by using the Born approximation, which consisted in two parts: the incident part and the contrast part. The possible solution in a Neumann series was outlined.

The incident wave, q_{inc}^i , belonging to the solution to the Fredholm integral equation turned out to be a convolution of the Green's function with a modified source F_d^i . Such convolution involved the existence of real and complex wave vectors k^i , and involved the problem to compute integrals with integrands containing gradients of variable density and combination of Hankel's functions. Anyhow, the analytic expressions for the incident pressure waves may be written as a functional part FP, and an integral part IP. Although similar approximations can be found in the literature (see [16]), we provided an approximated analytic solution for the incident wave and applied it to the problem of propagation of seismic waves.

Computational implementations were developed in order to compute, for different velocity profiles, the functional and the integral parts, which constitute the incident wave, q_{inc}^i . The computational analysis shows that the integral part is several orders of magnitude ($\sim 10^5$ times) smaller than its functional part and, therefore, the IP can be neglected, up to such precision degree.

The computational analysis allowed us to generate a simple formula to calculate the incident wave, which is involved in every term of the Neumann series expressing the solution of the pressure field of propagating waves in the medium with variable density. We claim that every application, in 2D, involving propagating waves, in a medium with variable density, can use this simple formula as long as such application allows for a solution in a Neumann series. The results presented herein motivate further exploration of the method to include higher-order terms in the expansion series such that we can include reflections and scattering of the wavefield, providing then a full description of wave phenomena in the medium. This issue is, nonetheless, out of the scope of this work and will be the object of future work.

The exploration of the modeling of waves to be implemented in a FWI process helped us understand the physical phenomena involved in the propagation of energy in a real medium. Such understanding leads us to conclude that a complete analytic solution of modeling is not possible in general and, consequently, iterative methods are required.

ACKNOWLEDGEMENTS

The authors would like to thank Dr. Carlos Piedrahíta and M.Sc. David Lambraño for invaluable discussions. This work is supported by ECOPETROL and COLCIENCIAS as part of the research project grant No. 0266-2013. Authors want to thank the referees for their observations and suggestions to the paper. JCMC thanks "Estrategia de Sostenibilidad, Universidad de Antioquia"

REFERENCES

- [1] J. Virieux, S. Operto, An overview of full-waveform inversion in exploration geophysics, *Geophysics*, 2009, 74 (6), WCC1-WCC26
- [2] Kapoor, S., Vigh, D., Li, H., Derharoutian, D. Full waveform inversion for detailed velocity model building, 74th, *EAGE Conference and Exhibition incorporating SPE EUROPEC 2012 Copenhagen, Denmark*, 4-7.
- [3] dos Santos, A. W. G. and Pestana, R.C. Time-domain multiscale full-waveform inversion using the rapid expansion method and efficient step-length estimation. *Geo-physics*, 2015, 80(4), R203-R216
- [4] Tao, Y., Sen, M. K., Frequency-domain full wave inversion with scattering-integral approach and its sensitivity analysis, *Journal of Geophysics and Engineering*. doi:10.1088/1742-2132/10/6/065008
- [5] Richards, Aki, (2009). *Quantitative Seismology*, University Science Books.
- [6] J. A. DeSanto, (1992), *Scalar Wave Theory Green's Functions Applications*, Springer.
- [7] P. D. Anno, A klein-gordon, (1993), *Acoustic theory*, Ph.D. thesis, Faculty in the Board of Trustees of the Colorado School of Mines.
- [8] Mavko, G. D. J., Mukerji T. (2009). *The Rock Physics Handbook*, Cambridge University Press.
- [9] Wang, Y. (2009). *Seismic Inverse Q Filtering*. Wiley. <https://doi.org/10.1029/2004GL020525>
- [10] A. D. Polyanin, (2002). *Handbook of Linear Partial Differential Equations for engineers and scientists*, Chapman and Hall.
- [11] J.-F. Treves, (1980). *Introduction to Pseudo-differential and Fourier Integral Operators: Pseudo-differential Operators*, University Series in Mathematics.
- [12] Barrett, K., Myers, H.H., (2004). *Foundations of Image Science*, Wiley,
- [13] P. M. van den Berg and R. E. Kleinman, (1997). "A contrast source inversion method," *Inverse Problems*, vol. 13, no. 6, pp. 1607-1620.
- [14] van den Berg, P. M., van Broekhoven, A. L., and Abubakar, A., Extended contrast source inversion, *Inverse Problems*, 1999,15, 1325-1343, <https://doi.org/10.1088/0266-5611/15/5/315>
- [15] Ramirez, A. B., van Dongen, K. W. A. Sparsity constrained Born inversion for breast cancer detection. doi:10.1109/ULTSYM.2015.0490
- [16] Ramirez, A. B. van Dongen, K. W. A. Sparsity constrained contrast source inversion, *J. Acoust. Soc. Am.* 2016. doi:10.1121/1.4962528
- [17] dos Santos, A. W. G., Pestana, R. C., Time-domain multiscale full-waveform inversion using the rapid expansion method and efficient step-length estimation, 2015, *Geophysics* 80 (4) R203-R216
- [18] Chen, G., Wu, R.-S., Chen, S. Full waveform inversion in time domain using time-damping filters, in: *SEG technical Program Expanded Abstracts, Society of Exploration Geophysicists*, 2015, pp. 1451-1455. doi:10.1190/segam2015-5878658.1
- [19] Murat Doğan a, Fatih Dikmen, Ali Alkumru, Line source diffraction by perfectly conducting successive steps, *Wave Motion*, 2017, (68) 253-271. <https://doi.org/10.1016/j.wavemoti.2016.10.004>
- [20] Versteeg, R. The marmousi experience: Velocity model determination on a synthetic complex data set, *The Leading Edge* (1994) 927-936
- [21] Jiménez, A. A. (2018). *Integral wave modelling and uncertainty quantification in full waveform inversion*, Ph.D. thesis, Universidad de Antioquia.